

Flavin containing monooxygenase 3 exerts broad effects on glucose and lipid metabolism and atherosclerosis^S

Diana M. Shih,* Zeneng Wang,[†] Richard Lee,[§] Yonghong Meng,* Nam Che,* Sarada Charugundla,* Hannah Qi,* Judy Wu,* Calvin Pan,* J. Mark Brown,[†] Thomas Vallim,* Brian J. Bennett,** Mark Graham,[§] Stanley L. Hazen,[†] and Aldons J. Lusis^{1,*†,§§}

Department of Medicine, Division of Cardiology,* and Departments of Human Genetics,^{††} and Microbiology, Immunology, and Molecular Genetics,^{§§}, David Geffen School of Medicine, University of California Los Angeles, Los Angeles, CA; Department of Cellular and Molecular Medicine (NC10),[†] Cleveland Clinic Lerner Research Institute, Cleveland, OH; Isis Pharmaceuticals,[§] Carlsbad, CA; and Department of Genetics,** University of North Carolina, Chapel Hill, NC

Abstract We performed silencing and overexpression studies of flavin containing monooxygenase (FMO) 3 in hyperlipidemic mouse models to examine its effects on trimethylamine *N*-oxide (TMAO) levels and atherosclerosis. Knockdown of hepatic FMO3 in LDL receptor knockout mice using an antisense oligonucleotide resulted in decreased circulating TMAO levels and atherosclerosis. Surprisingly, we also observed significant decreases in hepatic lipids and in levels of plasma lipids, ketone bodies, glucose, and insulin. FMO3 overexpression in transgenic mice, on the other hand, increased hepatic and plasma lipids. Global gene expression analyses suggested that these effects of FMO3 on lipogenesis and gluconeogenesis may be mediated through the PPAR α and Kruppel-like factor 15 pathways. In vivo and in vitro results were consistent with the concept that the effects were mediated directly by FMO3 rather than trimethylamine/TMAO; in particular, overexpression of FMO3 in the human hepatoma cell line, Hep3B, resulted in significantly increased glucose secretion and lipogenesis. **Our results indicate a major role for FMO3 in modulating glucose and lipid homeostasis in vivo, and they suggest that pharmacologic inhibition of FMO3 to reduce TMAO levels would be confounded by metabolic interactions.**—Shih, D. M., Z. Wang, R. Lee, Y. Meng, N. Che, S. Charugundla, H. Qi, J. Wu, C. Pan, J. M. Brown, T. Vallim, B. J. Bennett, M. Graham, S. L. Hazen, and A. J. Lusis. **Flavin containing monooxygenase 3 exerts broad effects on glucose and lipid metabolism and atherosclerosis.** *J. Lipid Res.* 2015. 56: 22–37.

Supplementary key words trimethylamine-*N*-oxide • peroxisome proliferator-activated receptor alpha • insulin

Flavin containing monooxygenase (FMO) 3 is an enzyme expressed primarily in the liver that catalyzes the

oxidation of trimethylamine (TMA) to trimethylamine-*N*-oxide (TMAO) (1). TMA is a gas that has a characteristic “fishy” odor that is produced entirely from the catabolism of dietary choline or carnitine by gut microbiota and then absorbed into the circulation (2, 3). Rare loss-of-function mutations of FMO3 have been shown to be a cause of “fish malodor syndrome” or trimethylaminuria, characterized by high levels of TMA (4–6). The incidence of trimethylaminuria caused by FMO3 mutations in Caucasian populations is estimated to be 1 in 10,000 (4). Some but not all trimethylaminuria patients have hypertension (6). However, common polymorphisms of the FMO3 gene are not associated with hypertension in the Caucasian population (7). To the best of our knowledge, whether loss-of-function FMO3 gene mutations influence metabolic traits such as plasma lipid, glucose, or insulin levels has not been reported. Recently, TMAO was shown to be significantly associated with coronary artery disease (CAD) in a large cohort of human subjects (3). A follow-up study confirmed

Abbreviations: Ad-CMV, control adenovirus; Ad-FMO3, adenovirus encoding the mouse FMO3; ALT, alanine aminotransferase; apoB Tg/HMDP, hybrid mouse diversity panel carrying a human apolipoprotein B transgene; Asbt, apical sodium dependent bile acid transporter; ASO, antisense oligonucleotide; AST, aspartate aminotransferase; CD68, cluster of differentiation 68; Cyp7a1, cytochrome P450, family 7, subfamily A, polypeptide 1; Cyp8b1, cytochrome P450, family 8, subfamily b, polypeptide 1; DE, differentially expressed; E3L, Apo-E Leiden; FGF, fibroblast growth factor; FMO, flavin containing monooxygenase; FOXO1, forkhead box O1; FPLC, fast-protein liquid chromatography; FXR, farnesoid X receptor; G6PC, glucose-6-phosphatase, catalytic subunit; HF/HC, high fat/high cholesterol; IL, interleukin; KLF15, Kruppel-like factor 15; LDLRKO, LDL receptor knockout; LXR, liver X receptor; PEPCK, phosphoenolpyruvate carboxykinase; PGC-1 α , peroxisome proliferator activated receptor γ coactivator protein-1 α ; SCD, stearoyl-CoA desaturase; SREBP-1c, sterol-regulatory element binding protein 1c; TC, total cholesterol; Tg, transgenic; TMA, trimethylamine; TMAO, trimethylamine-*N*-oxide.

To whom correspondence should be addressed.

e-mail: JLusis@mednet.ucla.edu

^S The online version of this article (available at <http://www.jlr.org>) contains supplementary data in the form of six tables and three figures.

This work was supported in part by National Institutes of Health Grants HL28481 and HL30568 (A.J.L., D.M.S.) and HL113452 (S.L.H.).

Manuscript received 10 June 2014 and in revised form 21 October 2014.

Published, JLR Papers in Press, November 6, 2014

DOI 10.1194/jlr.M051680

those original findings, showing that increased TMAO levels are associated with major adverse cardiovascular events, with a hazard ratio for the highest versus lowest quartile of 2.54 (8). The increased risk of CAD remained after adjustment for traditional risk factors. Furthermore, TMAO appears to be causal for the disease because in mice TMAO supplementation of the diet promoted atherosclerosis and antibiotic treatment, resulting in a block in TMA production, reduced atherosclerosis (2, 3). The mechanism by which TMAO contributes to disease is unknown, but some evidence points to altered cholesterol metabolism by macrophages (3) and diminished reverse cholesterol transport (2). Supporting the human results are genetic studies in natural variations of TMA and TMAO metabolism in populations of mice. Thus, in genetic crosses (3) or in surveys of inbred strains (1) of mice on hyperlipidemic backgrounds, TMAO levels were positively associated with atherosclerosis. A fraction of this variation was explained by genetic differences in FMO3 expression (1) and variations in gut microbiota composition also appear to contribute (9) (unpublished observations). These results raise the possibility that inhibition of FMO3 would lead to reduced levels of TMAO and retard the development of atherosclerosis.

We had previously shown in mice that second-generation antisense oligonucleotide (ASO)-mediated knockdown of hepatic FMO3 decreased TMAO levels and that overexpression of FMO3 using adenoviral transduction or transgenic (Tg) mice increased TMAO levels (1). In order to further examine how alterations in FMO3 contribute to atherosclerosis, we now report studies with mouse models of atherosclerosis, including the LDL receptor knockout (LDLRKO) mouse (10) and the Apo-E Leiden (E3L) Tg mice, another mouse model of hyperlipidemia (11). Our results confirm that knockdown of FMO3 decreased TMAO levels and atherosclerosis, but they also reveal unexpected effects on glucose and lipid metabolism. Our findings suggest that either FMO3 or TMA/TMAO has novel effects on metabolic functions. We show that FMO3 deficiency leads to decreased glucose and lipid levels in the circulation and in the liver, whereas FMO3 overexpression has opposite effects, indicating a role of FMO3 in modulating glucose and lipid homeostasis in vivo. Global gene expression and hepatic metabolite analyses suggest that these effects of FMO3 on glucose and lipid metabolism may be mediated through the PPAR α and Kruppel-like factor 15 (KLF15) pathways. Furthermore, studies in a hepatoma cell line in tissue culture suggest that the metabolic effects are mediated directly by FMO3 expression rather than by TMA/TMAO.

MATERIALS AND METHODS

ASO synthesis

A series of uniform chimeric 20-mer phosphorothioate oligonucleotides containing 2'-*O*-methoxyethyl groups at positions 1–5 and 15–20 targeted to murine FMO3, as well as a control ASO, were synthesized and purified on an automated DNA synthesizer using phosphoramidite chemistry as previously described (12).

Animals, diets, and study design

All animal experiments were approved by the University of California Los Angeles (UCLA) Animal Care and Use Committee, in accordance with Public Health Service guidelines. Eight-week-old female LDLRKO mice on a C57BL/6J background were purchased from the Jackson Laboratory. Beginning at 9 weeks of age, they were treated with a control ASO (ISIS 141923, 5'-CCTTCCCTGAAGGTTCCCTCC-3', 75 mg/kg body weight per week) or an FMO3-specific ASO (ISIS555847, 5'-TGGAAGCATTTGCCTTTAAA-3', 50 mg/kg body weight per week) through weekly intraperitoneal injection for a total of 13 injections. The mice were switched to a Western diet (Harlan TD.88137) during the last 8 weeks of the saline/ASO treatment to induce hyperlipidemia, a prerequisite for the development of significant atherosclerosis. At the end of the treatment period, the mice were fasted for 4 h before blood and tissues were collected for further analysis. For FMO3 ASO studies in C57BL/6J mice, 8-week-old female mice purchased from the Jackson Laboratory were treated with control ASO (ISIS 141923, 50 mg/kg body weight per week) or FMO3 ASO (ISIS 555847, 50 mg/kg body weight per week) through weekly intraperitoneal injection for a total of 13 (VLDL secretion study) or 5 (liver free fatty acid level determination study) injections, respectively. Five days after the last ASO injection, the mice were examined for VLDL-TG secretion rates or liver free fatty acid determination as described subsequently.

E3L Tg mice on a C57BL/6J background were a generous gift of Dr. L. Havekes (Leiden University Medical Center). FMO3 Tg mice (1) were crossed with the E3L Tg mice (11) to generate FMO3 Tg/E3L Tg and E3L Tg mice for the study. Because the ratio of human FMO3 mRNA level to mouse FMO3 mRNA level was much greater in male than female FMO3 Tg mice (data not shown), we chose to study the male FMO3 Tg mice so that the difference in FMO3 expression is greater between the Tg and non-Tg mice. Four-month-old male FMO3 Tg/E3L Tg and E3L Tg mice fed a low-fat chow diet were fasted for 4 h before collection of blood for plasma lipid analysis. The mice were then fed a high-fat (16% fat)/high-cholesterol (1% cholesterol) (HF/HC) diet (D10042101; Research Diets, New Brunswick, NJ) for 16 weeks and fasted for 16 h before blood and tissues were collected for further analysis.

Lipid, glucose, and bile acid analyses and liver toxicity markers

For plasma lipid, lipoprotein, and glucose level determinations, mice were fasted for 4 or 16 h before bleeding. Total cholesterol (TC), HDL cholesterol, unesterified/free cholesterol, TGs, free fatty acid, and glucose levels were determined by enzymatic colorimetric assays (13). Phosphatidylcholine levels were assayed using an enzymatic colorimetric assay from WAKO (Richmond, VA). Plasma alanine aminotransferase (ALT) and aspartate aminotransferase (AST) levels were determined using a clinical analyzer with reagents purchased from Beckman Coulter (Brea, CA). Total bile acids levels were assayed using a kit from Diazyme Laboratories (Poway, CA) according to the manufacturer's protocol. For lipid extraction, 50 mg of liver were homogenized in PBS, and the lipids then extracted using the Folch method (14). The extracted lipids were dried and resuspended in 1% Triton X-100 before lipid assays were performed as described previously. Plasma samples were fractionated by fast-protein liquid chromatography (FPLC) as described (15). Plasma concentrations of glucagon, interleukin (IL) 6, and insulin were determined by ELISA using kits from R and D systems (Minneapolis, MN), eBioscience (San Diego, CA), and ALPCO (Salem, NH), respectively.

Quantification of TMA, TMAO, bile acids, and free fatty acids by mass spectrometry

Quantification of TMAO and TMA in plasma samples was performed using stable isotope dilution HPLC with on-line electrospray ionization tandem mass spectrometry on an API 365 triple quadrupole mass spectrometer (Applied Biosystems, Foster, CA) interfaced with a Cohesive HPLC (Franklin, MA) equipped with phenyl column (4.6 × 2,505 mm, 5 μm Rexchrom Phenyl; Regis, Morton Grove, IL), and the separation was performed as reported previously (3).

Bile acid was extracted from small intestine and liver/gallbladder with ethanol as described by Argmann et al. (16). Bile acid internal standard mixture containing deoxycholic-2,2,4,4-d4 acid (C/D/N Isotopes cat. no. D-2941); cholic-2,2,4,4-d4 acid (C/D/N Isotopes cat. no. D-2452); glycochenodeoxycholic-2,2,4,4-d4 acid (C/D/N Isotopes cat. no. D-5673); and glycocholic-2,2,4,4-d4 acid (C/D/N Isotopes cat. no. D-3878) was added to the ethanolic extract at a final concentration of 10 μM each. Supernatants (20 μl) were analyzed by injection onto a Prodigy 5 u ODS (2) column (2.0 × 150 mm, 5 μm Luna silica, cat. no. 00F-3300-B0; Phenomenex, Torrance, CA) at a flow rate of 0.2 ml min⁻¹. Separation was performed using a discontinuous gradient generated by mixing solvent A (0.2% formic acid in water) with solvent B (0.2% formic acid in acetonitrile) at different ratios starting from 25% B for 5 min, then linearly to 100% B over 15 min, followed by 100% B for 5 min and then back to 25% B over 1 min. The HPLC column effluent was introduced into an API 365 triple quadrupole mass spectrometer with Ionics EP 10+ upgrade (Concord, Ontario, CA) interfaced to a Cohesive Technologies Aria LX Series HPLC multiplexing system. Analyses were performed using electrospray ionization in negative-ion mode with multiple reaction monitoring of parent and characteristic daughter ions specific for components monitored. The transitions monitored were *m/z*: *m/z* 391→345 for deoxycholic acid; *m/z* 395→349 for deoxycholic-2,2,4,4-d4 acid; *m/z* 407→371 for α-muricholic acid and β-muricholic acid; *m/z* 407→343 for cholic acid; *m/z* 411→347 for cholic-2,2,4,4-d4 acid; *m/z* 432→74 for glycolithocholic acid; *m/z* 448→74 for glycochenodeoxycholic acid, glycodeoxycholic acid, glycohyodeoxycholic acid, and glycooursodeoxycholic acid; *m/z* 452→74 for glycochenodeoxycholic-2,2,4,4-d4 acid; *m/z* 464→74 for glycocholic acid; *m/z* 468→74 for glycocholic-2,2,4,4-d4 acid; *m/z* 482→124 for tauroolithocholic acid; *m/z* 498→124 for taurochenodeoxycholic acid, taurodeoxycholic acid, taurohyodeoxycholic acid, and taurooursodeoxycholic acid; and *m/z* 514→124 for tauro-α-muricholic acid, tauro-β-muricholic acid, and taurocholic acid. Various concentrations of nonisotopically labeled bile acid standard mix were spiked into internal standard mix to prepare the calibration curves for quantification of individual bile acids. Deoxycholic-2,2,4,4-d4 acid was used as internal standard for deoxycholic acid; cholic-2,2,4,4-d4 acid for α-muricholic acid, β-muricholic acid, and cholic acid; glycochenodeoxycholic-2,2,4,4-d4 acid for glycochenodeoxycholic acid, glycodeoxycholic acid, glycohyodeoxycholic acid, and glycooursodeoxycholic acid; and glycocholic-2,2,4,4-d4 acid for all the other bile acid species.

Liver free fatty acids levels were quantified using mass spectrometry as previously described (17).

Quantification of enzymatic activity of FMOs in the liver

Quantification of enzymatic activity of hepatic FMOs was conducted in 250 μl reaction mix containing 1 mg liver protein homogenate, 100 μM d9-TMA, and 100 μM NADPH in 10 mM HEPES, pH 7.4. The reaction was stopped after 8 h with 0.2 N formic acid followed by filtering through a 3 K cutoff spin filter. The filtrate was injected onto an HPLC column with on-line tandem mass spectrometer to measure the oxidized product d9-TMAO (3).

VLDL-TG secretion assay

After 16 h fasting, plasma samples were collected from mice at baseline (time 0). The mice were then injected with poloxamer 407 (Sigma) intraperitoneally at a dose of 1 g/kg body weight. After 2 h, plasma samples were collected, and the mice were euthanized for tissue collection. Plasma TG levels at times 0 and 2 h were determined as described previously. The rate of VLDL-TG secretion was then calculated as described (18).

In vitro studies: adenovirus transduction, glucose secretion, and lipogenesis

Hep3B cells were cultured in MEM (Life Technologies, Carlsbad, CA) supplemented with 10% fetal bovine serum, 100 U/ml penicillin, 100 μg/ml streptomycin, and 1 mM sodium pyruvate. For the determination of glucose production, Hep3B cells were plated in a 6-well plate, at a density of 5 × 10⁵ cells/well. They were then infected with adenoviruses encoding mouse FMO3 (Ad-FMO3) or an empty vector (Ad-CMV) at multiplicity of infection (MOI) of 50 and cultured for 2 days. Afterwards, the cells were washed twice with PBS, then incubated with a glucose production media containing DMEM (no glucose), 4 mM L-glutamine, 20 mM sodium lactate, 2 mM sodium pyruvate, 100 U/ml penicillin, and 100 μg/ml streptomycin for 20 h before the conditioned media were collected for determination of glucose concentration by a PicoProbe™ Glucose Fluorometric Assay kit (BioVision, Milpitas, CA) according to the manufacturer's protocol. For the lipogenesis study, Hep3B cells were plated in a 24-well plate, at a density of 2 × 10⁵ cells/well and then infected with Ad-FMO3 or Ad-CMV at MOI of 50 and cultured for 2 days. Afterward, the cells were washed twice with PBS and incubated in 0.5 ml of growth media containing 2 μCi of ¹⁴C-acetate (50 mCi/mmol; American Radiolabeled Chemicals, St. Louis, MO) per well for 3 h before conditioned media, and cell lysate was collected for lipid extraction by the Folch method (14). The extracted lipids were spiked with unlabeled lipids (62.5 μg each of phospholipid, cholesterol, free fatty acid, TG, and cholesteryl ester), spotted on TLC plates (Silica Gel G plate, Alltech), and developed by petroleum ether-ethyl ether-acetic acid (84:15:1). Afterward, the lipid bands were stained with 2,7-dichlorofluorescein (Sigma) and visualized using a UV lamp. The ¹⁴C radioactivity associated with various lipid bands were scraped and counted by liquid scintillation counting (19). The lipid-associated radioactivity in cell lysate and conditioned media samples was normalized by the protein concentration of the cell lysate before comparison.

RNA isolation and quantitative RT-PCR analyses

Total RNA samples from tissues were isolated using Trizol reagent (Life Technologies) according to the manufacturer's protocol. The cDNA was synthesized using the High Capacity cDNA Reverse Transcription Kit (Applied Biosystems). Quantitative PCR was performed using gene-specific primers (supplementary Table 1) and the Roche SYBR green master mix in a Roche Lightcycler 480 system (Roche). The mRNA levels of specific genes were normalized to the mRNA levels of the housekeeping gene, Rpl13a, of the same sample.

Expression microarray

Total RNA samples from the livers of LDLRKO mice treated with control or FMO3 ASO (n = 4 for each group) were prepared for use in Illumina MouseRef-8 v2.0 Expression BeadChips according to manufacturer's recommendations at the Neuroscience Genomics Core at UCLA. Array data were processed using the limma R package; any probes that were not expressed (detection *P* value <0.05) in any of the arrays were excluded. Differential expression ratios were then calculated for the two groups (Control ASO vs. FMO3 ASO) and filtered at a 5% false discovery

rate cutoff. Fisher's exact test was performed to determine whether there is an enrichment of PPAR α target genes (20, 21) in the differentially expressed (DE) gene set.

Atherosclerosis lesion analyses

Atherosclerotic lesion size at the aortic root and proximal aorta was determined as described (13). Immunohistochemistry was performed, as previously described (22), using primary antibodies against cluster of differentiation 68 (CD68) (AbD Serotec, Raleigh, NC) to determine macrophage content of the aortic root lesion.

Statistical analyses

Student's *t*-test was utilized for comparison of means between two groups. In addition, ANOVA was used to compare means among three treatment groups. Values shown in bar graphs and tables are means and standard errors of the treatment groups. Biweight midcorrelation analysis was performed to examine the pair-wise relationships between plasma TMAO, HDL-cholesterol, VLDL/IDL/LDL-cholesterol levels, and atherosclerotic lesion size among 133 female mice that were bred onto a hyperlipidemic apoB Tg mouse background (apoB Tg/HMDP) (1, 23). Stepwise linear regression analysis was performed to examine the relative importance of TMAO, HDL-cholesterol, and VLDL/IDL/LDL-cholesterol in influencing atherosclerotic lesion size among 133 female apoB Tg/HMDP mice (1, 23).

RESULTS

FMO3 knockdown in vivo in LDLRKO mice: effects on TMA/TMAO and atherosclerosis

To examine how FMO3 expression influences atherogenesis, we administered saline, a control ASO, or an FMO3 ASO to LDLRKO mice for 13 weeks. During the last 8 weeks of the ASO treatment, the mice received a Western diet to enhance plasma cholesterol levels and atherosclerosis development. At the end of the study, the mice were euthanized and examined for plasma TMA/TMAO levels and atherosclerosis. We observed >90% reduction in FMO3 protein expression in the livers of the FMO3 ASO-treated mice as compared with the saline- and control ASO-treated mice (Fig. 1A). Liver FMO activity as measured by conversion of TMA to TMAO was decreased by 87% in the liver samples of FMO3 ASO-treated mice as compared with those of the control ASO group (Fig. 1B). Circulating TMAO levels in the FMO3 ASO-treated mice were decreased by about 50% as compared with the control ASO-treated mice (Fig. 1C), whereas circulating TMA levels were significantly increased in the FMO3 ASO-treated mice (Fig. 1D). While the FMO3 ASO treatment did not discernibly affect body weight as compared with the control groups (Fig. 1E), it did result in a small but significant reduction in weight of four major fat pads (Fig. 1F).

We observed a significant decrease in atherosclerotic lesion size at the aortic root of the FMO3 ASO group as compared with both the saline and the control ASO groups (Fig. 2A), whereas no difference in atherosclerotic lesion size was observed between the saline and control ASO groups (Fig. 2A). The macrophage content of lesions, as assessed by the relative area of CD68 staining, was similar (~70%) in all three groups (Fig. 2B).

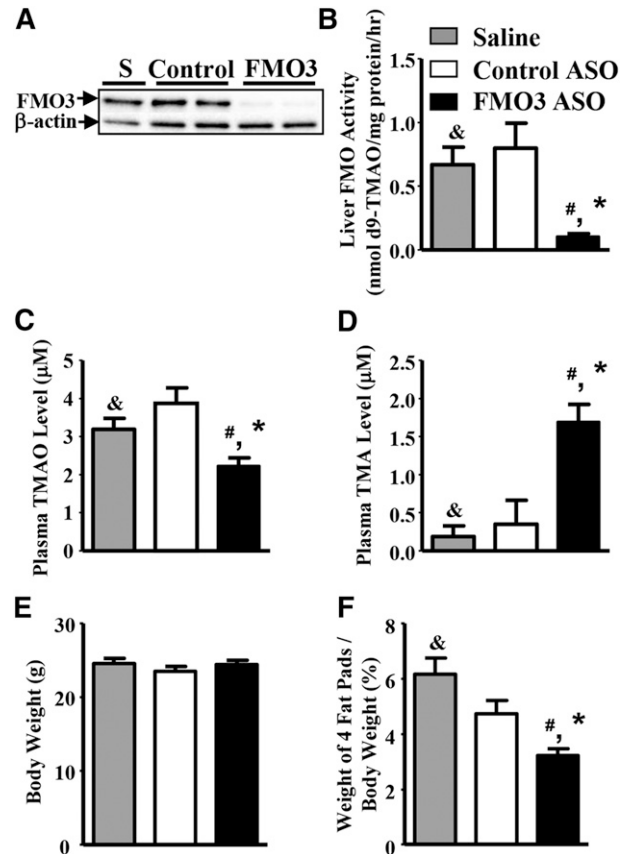


Fig. 1. FMO3 knockdown in LDLRKO mice leads to decreased hepatic FMO3 protein and activity levels, altered plasma TMAO and TMA levels, and decreased adiposity. A: Liver FMO3 protein levels of mice treated with saline (S), control ASO (control), or FMO3 ASO (FMO3) were determined by immunoblotting. B: Liver FMO activity ($n = 6$ for each group) was determined using TMA as the substrate. Plasma TMAO (C) and TMA (D) levels were determined by mass spectrometry ($n = 12$ for each group). Body weight (E) and percent weight of four fat pads (gonadal, retroperitoneal, subcutaneous, and mesentery fat pads) (F) were normalized by the body weight ($n = 12$ for each group). Student's *t*-test: # $P < 0.05$ as compared with the saline group; * $P < 0.05$ as compared with the control ASO group. ANOVA: &# $P < 0.05$ between the means of the three treatment groups.

FMO3 knockdown results in altered levels of plasma lipoproteins and insulin in LDLRKO mice fed a Western diet

Mice injected with the FMO3 ASO exhibited dramatically decreased levels of plasma lipids, including TG, HDL, VLDL/IDL/LDL, unesterified cholesterol, and free fatty acids, as compared with mice treated with the control ASO (Table 1). The control ASO had a slight effect on plasma TG levels and HDL cholesterol levels but did not affect the other lipids (Table 1). These results were consistent with FPLC analyses, which revealed decreased levels of TG, TC, and phosphatidylcholine in the VLDL and IDL/LDL fractions of the FMO3 ASO plasma samples as compared with those of the control ASO samples (Fig. 3A–C). Decreased levels of TC and phosphatidylcholine were also observed in the HDL fractions of the FMO3 ASO plasma samples (Fig. 3B, C). Bile acids were elevated about 2-fold in the FMO3 ASO-injected mice (Fig. 4C). In addition to these

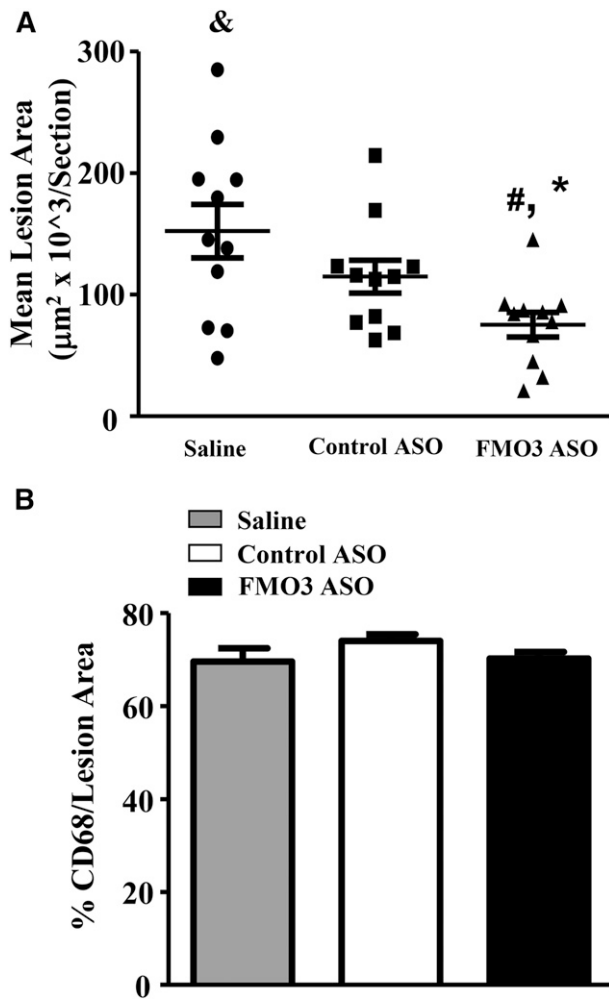


Fig. 2. FMO3 knockdown in LDLRKO mice leads to decreased atherosclerotic lesion development. **A:** Atherosclerotic lesion size at the aortic root region of mice treated with saline, control ASO, or FMO3 ASO and fed the Western diet are shown. $N = 11$ for each group. Symbols are the same as Fig. 1. **B:** Macrophage content in the atherosclerotic lesions of the aortic root region was determined by immunohistochemistry using antibodies against CD68. Four mice from each group with three lesion sections per mouse were used in the comparison.

effects, the FMO3 ASO-treated mice also exhibited significant decreases in both glucose and insulin levels as compared with the control ASO treated mice (Table 1).

To evaluate the potential toxic effects of FMO3 ASO treatment, we measured plasma ALT and AST levels as biomarkers for normal liver function. Although levels were elevated about 2-fold in the FMO3 ASO-treated mice as compared with the control ASO-treated mice (Fig. 4A, B), they did not exceed the normal ranges previously reported for untreated LDLRKO (15) and C57BL/6 mice (24). Further, circulating levels of a proinflammatory cytokine, IL-6, were similar between the FMO3 ASO-treated mice and the saline- and control ASO-treated mice (Fig. 4E). Circulating levels of urea, a metabolite mainly produced by the liver, were significantly decreased in the FMO3 ASO-injected mice as compared with the saline- and control ASO-treated mice (Fig. 4D). Thus, FMO3 knockdown in

TABLE 1. Plasma lipid, lipoprotein, glucose, and insulin levels of female LDLRKO mice maintained on a Western diet with various treatments

Treatment	n	TGs	TC	HDL Cholesterol	VLDL/IDL/LDL Cholesterol	Unesterified Cholesterol	Free Fatty Acids	Glucose	Insulin
Saline	12	301 (29)	1,302 (74)	79 (3)	1,223 (72)	415 (23)	38 (2)	307 (21)	307 (43)
Control ASO	12	429 (34) ^a	1,282 (46)	91 (3) ^a	1,191 (45)	404 (14)	42 (3)	350 (13)	353 (40)
FMO3 ASO	12	66 (5) ^{a,b}	332 (23) ^{a,b}	43 (3) ^{a,b}	289 (21) ^{a,b}	102 (7)	24 (1) ^{a,b}	267 (12) ^b	146 (25) ^{a,b}

Mice were fasted for 4 h. Values shown are means (standard errors) of the groups. Units are mg/dl except insulin, for which the unit is pg/ml. ANOVA was also performed to analyze the differences between the three group means with all traits exhibiting P -values < 0.05 .

^aStudent's t -test: $P < 0.05$ versus saline.

^bStudent's t -test: $P < 0.05$ versus control ASO.

mice is associated with changes in the levels of plasma lipoproteins, glucose, and insulin, without significant impairment in liver function.

FMO3 knockdown alters hepatic lipid and glucose metabolism

We observed significantly decreased levels of TGs, TC, and phosphatidylcholine in the livers of FMO3 ASO-injected mice as compared with those of the saline- and control ASO-treated mice (Fig. 5A–C), whereas control ASO-injected mice were unaffected in hepatic lipids except for a small decrease in liver TG content as compared with the saline group (Fig. 5A). Liver glucose levels in the FMO3 ASO-injected mice were significantly lower as compared with the control ASO group (Fig. 5D), while liver glycogen levels of the FMO3 ASO and control ASO groups were both slightly elevated as compared with the saline group (Fig. 5E).

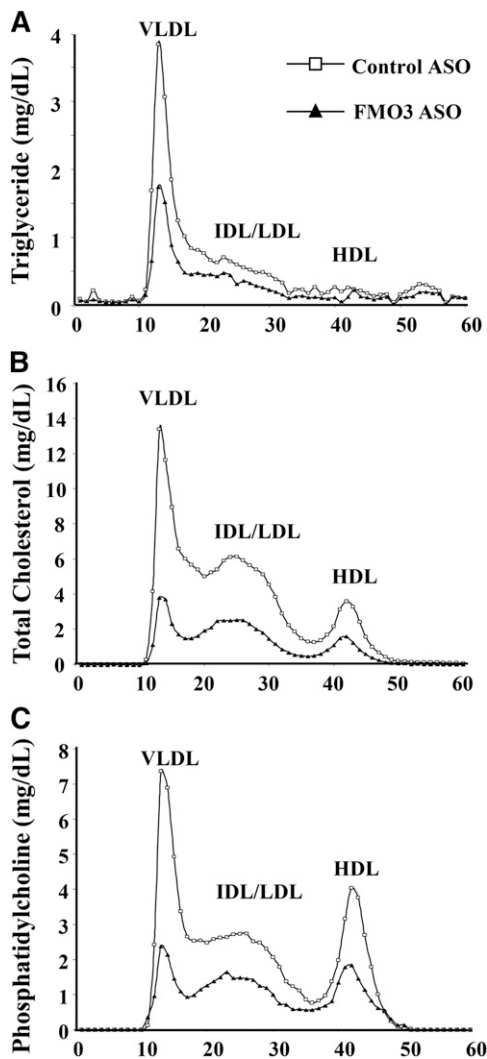


Fig. 3. Altered plasma lipoprotein profile in FMO3 ASO-treated LDLRKO mice fed a Western diet. FPLC was used to fractionate pooled plasma samples (five individual samples per pool) from LDLRKO mice treated with the control ASO or the FMO3 ASO and fed the Western diet. TG (A), TC (B), and phosphatidylcholine (C) concentrations of each FPLC fraction were measured and shown.

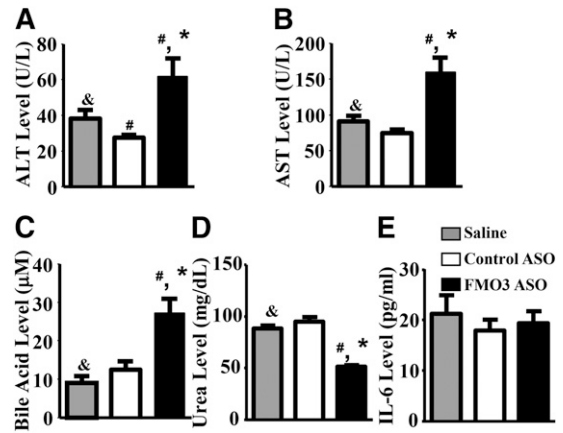


Fig. 4. FMO3 knockdown in LDLRKO mice is associated with increased levels of hepatotoxicity markers and bile acids and decreased levels of urea in the blood. Plasma ALT (A), plasma AST (B), plasma total bile acid (C), plasma urea (D), and plasma IL-6 (E) concentrations are shown. For A–E, n = 10 to 12 per group. Symbols are the same as in Fig. 1.

To examine the effects of the ASO on hepatic gene expression, we performed quantitative RT-PCR. We observed significantly decreased expression of several genes involved in lipogenesis, including sterol-regulatory element binding protein 1c (*Srebp-1c*), fatty acid synthase (*Fasn*), malic enzyme (*Me*), stearoyl-CoA desaturase-1 (*Scd-1*), and ELOVL family member 6, elongation of long chain fatty acids (*Elovl6*) in the livers of FMO3 ASO-treated mice as compared with those of the control ASO group (Fig. 5F). These data provided a potential mechanism for reduced hepatic TG and phosphatidylcholine levels found in the FMO3 ASO-treated group as compared with the control ASO-treated group. The mRNA level for microsomal TG transfer protein (*Mttp*) was significantly decreased in the FMO3 ASO-treated group as well (Fig. 5F), providing an explanation for decreased VLDL levels seen in these mice (Fig. 3). Significant decreases in the expression of genes involved in gluconeogenesis or its regulation, such as *Alt*, fibroblast growth factor 21 (*Fgf21*), peroxisome proliferator activated receptor γ coactivator protein-1 α (*Pgc-1 α*), forkhead box O1 (*Foxo1*), glucose-6-phosphatase, catalytic subunit (*G6pc*), pyruvate dehydrogenase kinase, isozyme 4 (*Pdk4*), and phosphoenolpyruvate carboxykinase (*Pepck*) were also observed in FMO3 ASO group as compared with the control ASO group (Fig. 5F). These transcriptional changes may explain, in part, the decreased plasma and hepatic glucose levels observed in the FMO3 ASO-treated group. The mRNA levels of genes involved in fatty acid oxidation, such as acyl-CoA dehydrogenase, long-chain (*Acadl*) and enoyl-CoA hydratase/3-hydroxyacyl CoA dehydrogenase (*Ehhadh*) were also significantly decreased in the FMO3 ASO-treated group (Fig. 5F).

PPAR α and KLF15 pathways perturbed by FMO3 knockdown

Because substantial decreases in mRNA levels of many genes involved in glucose and lipid metabolism were

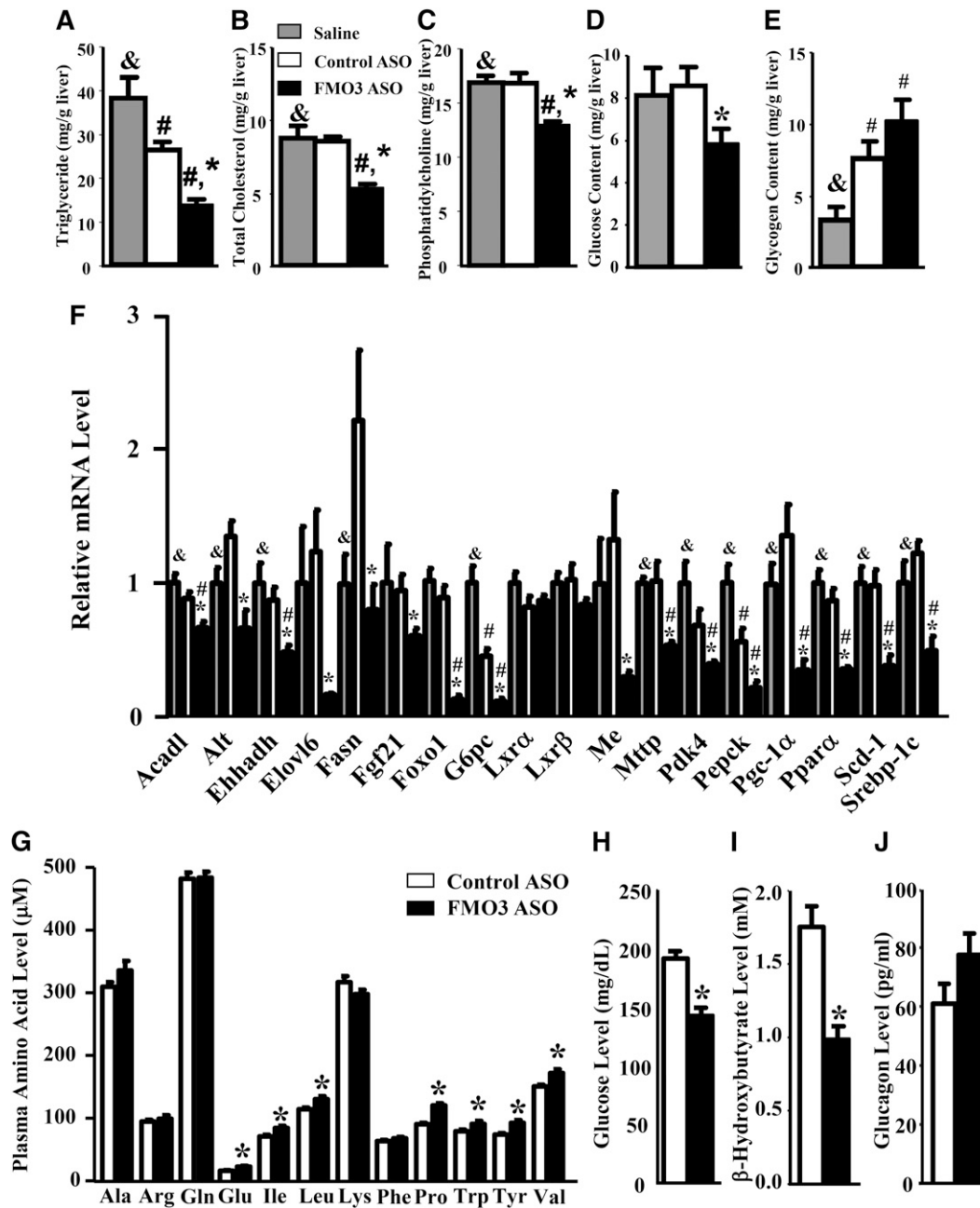


Fig. 5. FMO3 knockdown in LDLRKO mice leads to altered hepatic glucose and lipid levels, altered hepatic gene expression, and changes in plasma metabolites. Liver TG (A), TC (B), phosphatidylcholine (C), glucose (D), and glycogen (E) levels were determined in LDLRKO mice treated with saline, control ASO, or FMO3 ASO and fed the Western diet ($n = 8$ for each group). F: Liver mRNA levels ($n = 6$ for each group) of genes involved in lipid and glucose metabolism were quantified by quantitative PCR and normalized by the mRNA level of the housekeeping gene, *Rpl13a*. In a separate set of mice, circulating levels of amino acids (G), glucose (H), β -hydroxybutyrate (I), and glucagon (J) were determined ($n = 10$ for each group). Symbols are the same as in Fig. 1.

observed in the FMO3 ASO-treated group, we asked whether the expression levels of transcription factors regulating these processes, including liver X receptor (LXR) α , LXR β , and PPAR α , were altered in these mice. Our data showed that the expression of LXR α and LXR β was not changed in the FMO3 ASO-treated group, whereas PPAR α mRNA levels were significantly decreased in the FMO3 ASO-treated group (Fig. 5F). Global gene expression profiling analysis was performed to identify DE liver genes

between the control ASO- and FMO3 ASO-treated groups. Overall, 27% of the liver transcripts (4,223 out of 15,552) were DE between the two groups with about 50% of the DE transcripts upregulated and the other 50% downregulated. In contrast, out of 331 PPAR α target genes, 156 of those (47%, 136 downregulated and 20 upregulated) were DE between FMO3 ASO- and control ASO-treated groups (supplementary Table 2). Thus, we observed an enrichment of PPAR α target genes in the DE gene set (Fisher's

exact test, $P = 3.6 \times 10^{-15}$). Furthermore, 87% (136 out of 156) of the DE PPAR α target genes versus 50% of transcripts of the overall DE gene set were downregulated in the FMO3 ASO groups (Fisher's exact test, $P = 2.7 \times 10^{-23}$). Therefore, our data show that FMO3 knockdown preferentially decreased PPAR α target gene expression in the liver. Our results suggest that FMO3 may influence lipid and glucose metabolism through modulating PPAR α expression and activity.

To further examine why FMO3 knockdown leads to decreased levels of circulating and hepatic glucose in LDLRKO mice, we examined the circulating levels of 12 amino acids that are glucogenic and/or ketogenic in a second set of mice that received either control or FMO3 ASO treatment. Interestingly, the levels of 7 out of these 12 amino acids examined, namely, Glu, Ile, Leu, Pro, Trp, Tyr, and Val, were significantly elevated, by 14% to 38%, as compared with those of the control ASO-treated mice (Fig. 5G). Plasma glucose and β -hydroxybutyrate (a ketone body produced by the liver) in these FMO3 ASO-treated mice were also significantly lower as compared with the control ASO-treated mice (Fig. 5H, I). We noticed that plasma glucose levels (Fig. 5H) of this second set of mice, housed at UCLA, were generally lower than those of the first set of mice, housed at ISIS (Table 1), although both experiments used similar study protocols [LDLRKO females, Western diet, same ASOs, and same duration of fasting (4 h)]. However, differences in the environment, animal handling, and stress levels of the mice could all contribute to the differences in plasma glucose levels observed between these two cohorts of mice. Our data suggest decreased hepatic gluconeogenesis and ketone body production in the FMO3 ASO-treated mice as compared with the control ASO-treated mice. However, circulating glucagon levels were similar between the FMO3 ASO- and control ASO-treated mice (Fig. 5J), indicating that the decreased hepatic expression of gluconeogenic genes in the livers of FMO3 ASO-treated mice (Fig. 5F) was not due to decreased glucagon stimulation. On the other hand, *Fgf21* and *Pgc-1 α* mRNA levels were significantly decreased in the FMO3 ASO-treated group (Fig. 5F). *FGF21* is a PPAR α target gene that induces *PGC-1 α* expression, leading to increased gluconeogenesis and ketogenesis (25). Therefore, decreased *FGF21* and *PGC-1 α* expression in the liver may be one of causes leading to decreased plasma glucose and ketone levels observed in the FMO3 ASO-treated mice.

The *Klf15* is a transcription factor that regulates gluconeogenesis, amino acid degradation, and urea cycle in the liver (26–28). Our liver microarray data revealed significant decreases in the mRNA levels of *Klf15* and some of its target genes including *G6c*, *Pck1*, ornithine transcarbamylase (*Otc*), *Prodh*, and *Hpd* in the FMO3 ASO-treated group (supplementary Table 3). The decreased expression of *Klf15* and its target genes could also explain, at least in part, the decreased plasma and liver glucose levels, decreased plasma urea level, and increased plasma gluconeogenic amino acid levels seen in the FMO3 ASO-treated mice.

FMO3 knockdown alters bile acid metabolism, fecal lipid content, and intestinal gene expression

Because the substrate for FMO3, TMA, is produced by gut microbiota, we asked whether the lower plasma and hepatic lipid levels might be mediated by bile acid metabolism, intestinal cholesterol absorption, or TG digestion. Bile samples collected from the gall bladders of FMO3 ASO-treated mice exhibited significantly lower levels of cholesterol, bile acids, and phosphatidylcholine as compared with those of the saline- and control ASO-treated mice (Fig. 6A). FMO3 ASO-treated mice exhibited significantly decreased bile acid pool size as compared with the control ASO group (Fig. 6B, left panel). The levels of various bile acids, including cholate, taurocholate, taurochenodeoxycholate, tauro- α -muricholate, taurodeoxycholate, and tauroursodeoxycholate, were significantly decreased by >50% in the liver/gallbladder of FMO3 ASO-treated mice (Fig. 6B, middle panel). The levels of taurochenodeoxycholate, tauro- α -muricholate, taurodeoxycholate, and tauroursodeoxycholate were significantly decreased in the small intestine of the FMO3 ASO-treated mice as well (Fig. 6B, right panel). Interestingly, two major bile acids, taurocholic acid and tauro- β -muricholic acid, were increased in both the control ASO and FMO3 ASO groups as compared with the saline group in the small intestine (Fig. 6B, right panel). This might be caused by a nonspecific effect of the ASO in general. Hepatic mRNA levels of enzymes involved in bile acid synthesis [including cytochrome P450, family 7, subfamily A, polypeptide 1 (*Cyp7a1*); cytochrome P450, family 8, subfamily b, polypeptide 1 (*Cyp8b1*); and cytochrome P450, family 27, subfamily A, polypeptide 1 (*Cyp27a1*)] were all significantly reduced in the FMO3 ASO-treated mice (Fig. 6C), suggesting that lower hepatic bile acid synthesis may account for the lower bile acid concentrations found in the bile, liver, and small intestine of these mice. Hepatic mRNA levels of the bile acid transporter, Na/taurocholate cotransporting polypeptide 1 (*Ntcp*), were also lower in the FMO3 ASO-treated mice (Fig. 6C). This might also explain the higher circulating bile acid levels observed in these mice. We also observed increased inflammation in the livers of FMO3 ASO-treated mice as evidenced by increased mRNA levels for *Cd68*, a marker for macrophages, and tumor necrosis factor α (*Tnf α*) (Fig. 6C). The cholesterol content of the fecal samples collected from the FMO3 ASO-treated mice were significantly higher as compared with those of saline- and control ASO-treated mice (Fig. 6D), indicating either lower intestinal cholesterol absorption or increased cholesterol excretion in the FMO3 ASO-treated mice. Fecal TG contents, on the other hand, were not affected by the FMO3 ASO treatment (Fig. 6D). We further examined gene expression in the small intestine of these mice. Interestingly, the mRNA levels of Niemann-Pick C1-like 1 (*Npc1l1*), a key player in intestinal cholesterol absorption, were significantly lower in the FMO3 ASO-treated mice (Fig. 6E), which may explain, in part, the increased fecal cholesterol levels seen in the FMO3 ASO-treated mice. The mRNA levels of the cholesterol transporters, *Abcg5* and *Abcg8*, were also decreased in the FMO3 ASO-treated mice

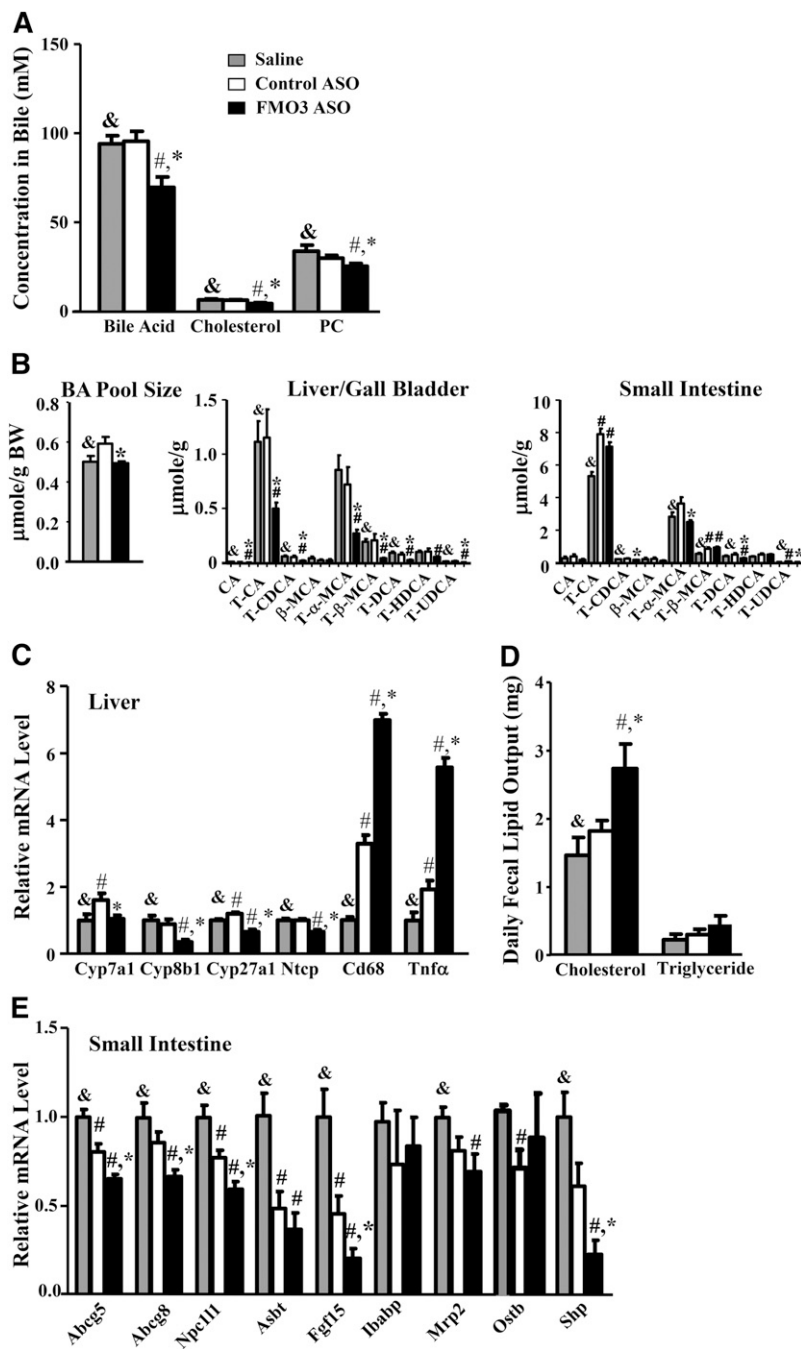


Fig. 6. FMO3 knockdown in LDLRKO mice leads to altered bile composition, bile acid pool size, fecal lipid output, and intestinal gene expression. Bile acid, cholesterol, and phosphatidylcholine (PC) levels of bile collected from the gall bladder (A), bile acid (BA) pool size and composition (B) [for bile acid composition, only the major ($\geq 0.5\%$ of total amount) bile acid species are plotted], hepatic mRNA levels (C), daily fecal output of cholesterol and TG (D), and mRNA levels (E) in the small intestine of LDLRKO mice treated with saline, control ASO, or FMO3 ASO were determined ($n = 6$ for each group). Symbols are the same as in Fig. 1. CA, cholic acid; CDCA, chenodeoxycholic acid; DCA, deoxycholic acid; HDCA, hydoxycholic acid; MCA, muricholic acid; T, taurine conjugated; UDCA, ursodeoxycholic acid.

as compared with the saline- and control ASO-treated mice (Fig. 6E). The mRNA levels of two farnesoid X receptor (Fxr) target genes, fibroblast growth factor 15 (*Fgf15*) and small heterodimer partner (*Shp*), were also significantly decreased in the FMO3 ASO-treated mice (Fig. 6E), suggesting decreased intestinal bile acid levels in the FMO3 ASO-treated mice. The mRNA levels of genes involved in bile acid transport, including apical sodium dependent bile acid transporter (*Asbt*), intestinal bile acid binding protein (*Ibabp*), multidrug resistance-associated protein 2 (*Mrp2*), and organic solute transporter β (*Ostb*), were similar between the FMO3 ASO and control ASO groups (Fig. 6E), providing indirect evidence that FMO3 knockdown did not directly affect bile acid transport in the intestine.

FMO3 knockdown results in altered plasma lipoprotein, glucose, and insulin levels and decreased hepatic VLDL-TG secretion in nonhyperlipidemic genetic background

We examined the effects of FMO3 knockdown in a separate cohort of female C57BL/6J (B6) mice injected with either control or FMO3 ASO for 13 weeks while maintained on a low-fat chow diet. B6 mice injected with the FMO3 ASO showed significant decreases in plasma TGs, HDL, and unesterified cholesterol levels as compared to the control ASO-treated mice (Table 2). The FMO3 ASO-treated mice also exhibited significant decreases in both glucose and insulin levels as compared with the control ASO-treated mice (Table 2). Hepatic TG levels were significantly decreased in the FMO3 ASO-treated group (Fig. 7A), and this was

TABLE 2. Plasma lipid, lipoprotein, glucose, and insulin levels of female B6 mice injected with control or FMO3 ASO and maintained on a chow diet

Treatment	n	TG	TC	HDL Cholesterol	VLDL/IDL/LDL Cholesterol	Unesterified Cholesterol	Free Fatty Acids	Glucose	Insulin
Control ASO	8	103 (24)	93 (4)	64 (3)	28 (2)	14 (1)	55 (7)	130 (8)	260 (49)
FMO3 ASO	8	50 (11) ^a	70 (5) ^a	50 (5) ^a	21 (2)	11 (1) ^a	50 (5)	111 (6) ^a	136 (13) ^a

Mice were fasted for 16 h. Values shown are means (standard errors) of the groups. Units are mg/dl except insulin, for which the unit is pg/ml. ^a $P < 0.05$ versus control ASO.

accompanied by a small but significant increase in TC level (Fig. 7A). No differences in phosphatidylcholine levels were observed between the two groups of mice (Fig. 7A). FMO3 ASO-treated mice exhibited a significant 20% decrease in TG secretion rate as compared with the control mice (Fig. 7B), suggesting that the decreased plasma TG levels observed in the FMO3 ASO-treated mice (Table 2) were caused, in part, by decreased TG secretion from the liver.

In a second study, saturated and unsaturated fatty acids in the liver samples of female C57BL/6J mice injected with either control or FMO3 ASO for 5 weeks were quantified by mass spectrometry. We observed no significant differences in most of the saturated fatty acids measured, except for decreased caproate and myristate levels in the FMO3 ASO group (Fig. 7C). In contrast, hepatic levels of most of the unsaturated fatty acids, including palmitoleate, oleate, α -/ γ -linolenate, and EPA, were significantly decreased in the FMO3 ASO-treated group as compared with the control ASO group (Fig. 7D). Because many unsaturated fatty acids are known PPAR α ligands (21), the decreased levels of unsaturated fatty acids observed in the livers of FMO3 ASO-treated mice may explain the

decreased hepatic expression of PPAR α target genes associated with FMO3 knockdown (supplementary Table 2).

FMO3 knockdown using a second FMO3 ASO results in altered plasma lipoprotein, glucose, and insulin levels

To rule out the possibility that the lipid- and glucose-lowering effect of the FMO3 ASO used in the LDLRKO and B6 mouse studies described previously was due to a nonspecific effect, we examined the effect of a second FMO3 ASO (FMO3 ASO#2, ISIS 555926) on plasma lipid and glucose levels in B6 mice. After six weekly ASO injections, male B6 mice treated with the FMO3 ASO#2 showed significant decreases in plasma TGs, total, HDL, and unesterified cholesterol levels as compared with the control ASO-treated mice (supplementary Table 4). The FMO3 ASO#2-treated mice also exhibited significant decreases in both glucose and insulin levels as compared with the control mice (supplementary Table 4). Thus, FMO3 knockdown using two independent FMO3 ASOs in vivo yielded reproducible lipid- and glucose-lowering effects, indicating a role for FMO3 in lipid and glucose homeostasis.

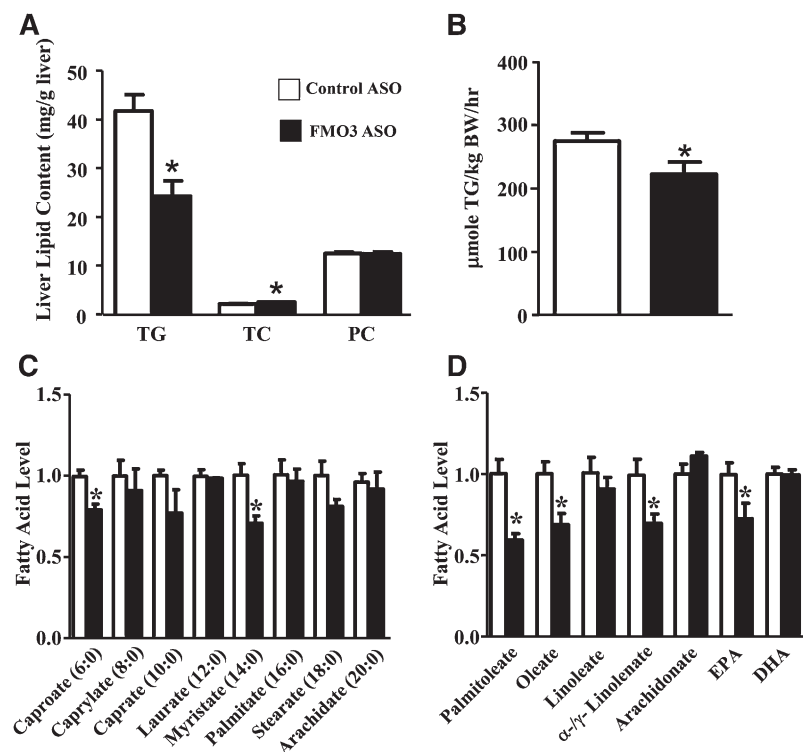


Fig. 7. FMO3 knockdown in C57BL/6J mice fed a chow diet leads to decreased liver TG and fatty acid concentrations and a decreased rate of secretion of VLDL-TG. Female C57BL/6J mice were treated with control or FMO3 ASO for 13 weeks before liver concentrations of TG, TC, and phosphatidylcholine (PC) (A), and the rate of VLDL-TG secretion (B) were determined (n = 8 for each group). In a separate study, the levels of saturated fatty acids (C) and unsaturated fatty acids (D) in the livers of C57BL/6J mice treated with five weekly injections of control or FMO3 ASO were determined by mass spectrometry (n = 4 for each group). Student's *t*-test: * $P < 0.05$ as compared with the control ASO group.

Overexpression of human FMO3 in Tg mice results in altered plasma lipoprotein, glucose, and insulin levels; altered hepatic lipid contents; and increased adiposity

We examined FMO3 Tg mice to determine whether FMO3 overexpression also has an impact on plasma lipids and glucose metabolism. We previously reported the generation of FMO3 Tg mice overexpressing human FMO3 from a liver-specific albumin promoter (1). The male FMO3 Tg mice exhibited a significant 55% increase in liver FMO activity (supplementary Fig. 1) and a significant 75% increase in plasma TMAO levels as compared with the male non-Tg littermates when the mice were supplemented with water containing 1.3% choline chloride (supplementary Fig. 1).

We introduced the FMO3 transgene on to a hyperlipidemic mouse model, the E3L Tg mouse (11) for further analysis. The E3L Tg was chosen because it shows a dominant effect with respect to hypercholesterolemia, in contrast to the LDLRKO model, and thus reduces the breeding required for generation of the FMO3 Tg mice on a hyperlipidemic background. When fed either low-fat chow or HF/HC diets, the FMO3 Tg/E3L Tg mice exhibited significantly increased plasma TG, VLDL/IDL/LDL, and unesterified cholesterol as compared with the E3L Tg mice (Table 3), consistent with the ASO experiments, which had the opposite effects. We also observed increased glucose and insulin levels in the FMO3 Tg mice (Table 3; $P \leq 0.1$). No significant changes in HDL cholesterol or free fatty acid levels were observed between these two groups of mice fed the same diet (Table 3). FPLC analysis of plasma lipoproteins revealed increased levels of TG, TC, and phosphatidylcholine in the VLDL fractions of the FMO3 Tg plasma samples as compared with those of the E3L Tg samples (supplementary Fig. 2A–C) from mice fed the HF/HC diet. Increased levels of TC and phosphatidylcholine were also observed in the IDL/LDL fractions of the FMO3 Tg plasma samples (supplementary Fig. 2B, C). No changes in TC or phosphatidylcholine levels were observed between the HDL fractions of the two groups (supplementary Fig. 2B, C).

When fed an HF/HC diet, the FMO3 Tg/E3L Tg mice exhibited a 40% increase in liver FMO activity ($P = 0.08$) as compared with the E3L Tg mice (Fig. 8A, left panel). There was a trend of increased circulating TMAO levels ($P = 0.09$) in the FMO3 Tg/E3L Tg mice as compared with the E3L Tg mice (Fig. 8A, right panel), whereas circulating

TMA levels were similar between the two groups (Fig. 8A, right panel). We also observed increased TG accumulation in the livers of FMO3 Tg mice (Fig. 8B), although hepatic TC and phosphatidylcholine levels were similar between the two groups (Fig. 8B). There was a significant 10% increase in overall bile acid pool size in the FMO3 Tg/E3L Tg mice as compared with the E3L Tg mice (Fig. 8C, left panel). The hepatic concentrations of various bile acids were similar between the FMO3 Tg/E3L Tg and E3L Tg mice except for a small but significant decrease in tauroursodeoxycholate level in the FMO3 Tg/E3L Tg mice (Fig. 8C, middle panel). There were significant increases in taurochenodeoxycholate (54% increase) and tauro- β -muricholate (31% increase) levels in the small intestine of FMO3 Tg/E3L Tg mice (Fig. 8C, right panel). Hepatic gene expression analysis revealed no significant differences in mRNA levels of genes involved in lipid, glucose, bile acid, or cholesterol metabolism between the FMO3/E3L Tg and E3L Tg mice (supplementary Fig. 3A). Gene expression analysis of the small intestine revealed a significant decrease in *Asbt* mRNA level in the FMO3 Tg/E3L Tg mice (supplementary Fig. 3B), whereas no other changes in the expression of genes involved in cholesterol and bile acid transport were observed. *Asbt* is the major bile salt uptake protein in the small intestine. FXR is shown to inhibit the expression of mouse *Asbt* via the FXR-SHP-liver receptor homolog-1 cascade (29). Because the FMO3 Tg/E3L Tg mice had a significant 54% increase in taurochenodeoxycholate, a potent FXR ligand, in the small intestine, this may explain the decreased *Asbt* expression in these mice. In addition, FMO3 Tg mice exhibited significantly increased body weight (Fig. 8D) and adiposity (Fig. 8E) after the HF/HC diet feeding. There was a small increase (20%) in atherosclerotic lesion size in the FMO3 Tg/E3L Tg mice (vs. E3L Tg, $P = 0.23$; Fig. 8F). Therefore, data from the FMO3 Tg mice support a role for FMO3 in glucose, lipid homeostasis, and adiposity.

Overexpression of FMO3 in Hep3B cells enhances lipogenesis and glucose production

To further examine the effect of FMO3 on lipid and glucose metabolism, we infected the human Hep3B hepatoma cells with control (Ad-CMV) or mouse FMO3-encoding adenoviral vectors (1). Forty-eight hours after infection, we observed high levels of FMO3 protein being expressed in the Ad-FMO3-infected cells as compared with the

TABLE 3. Plasma lipid, lipoprotein, glucose, and insulin levels of FMO3 Tg/E3L Tg and E3L Tg mice maintained on chow or HF/HC diets

Genotype	Diet	n	TG	TC	HDL Cholesterol	VLDL/IDL/LDL Cholesterol	Unesterified Cholesterol	Free Fatty Acids	Glucose	Insulin
E3L Tg	Chow	8	104 (13)	93 (9)	48 (10)	45 (5)	29 (3)	36 (2)	182 (13)	852 (172)
FMO3 Tg/E3L Tg	Chow	12	148 (8) ^a	115 (6) ^a	51 (4)	64 (5) ^a	37 (2) ^a	38 (2)	205 (4) ^b	1,454 (222) ^b
E3L Tg	HF/HC	9	438 (71)	702 (92)	87 (3)	616 (94)	243 (43)	44 (2)	139 (15)	912 (240)
FMO3 Tg/E3L Tg	HF/HC	13	619 (53) ^a	916 (44) ^a	95 (4)	821 (44) ^a	335 (19) ^a	37 (3)	164 (7) ^b	981 (65) ^c

Mice fed the chow diet were fasted for 4 h. Mice fed the HF/HC diet were fasted for 16 h. Values shown are means (standard errors) of the groups. Units are mg/dl except insulin, for which the unit is pg/ml.

^a $P \leq 0.05$ versus E3L Tg of the same diet.

^b $P < 0.1$ versus E3L Tg of the same diet.

^cNatural log-transformed data were used for comparison; $P = 0.1$ versus E3L Tg of the same diet.

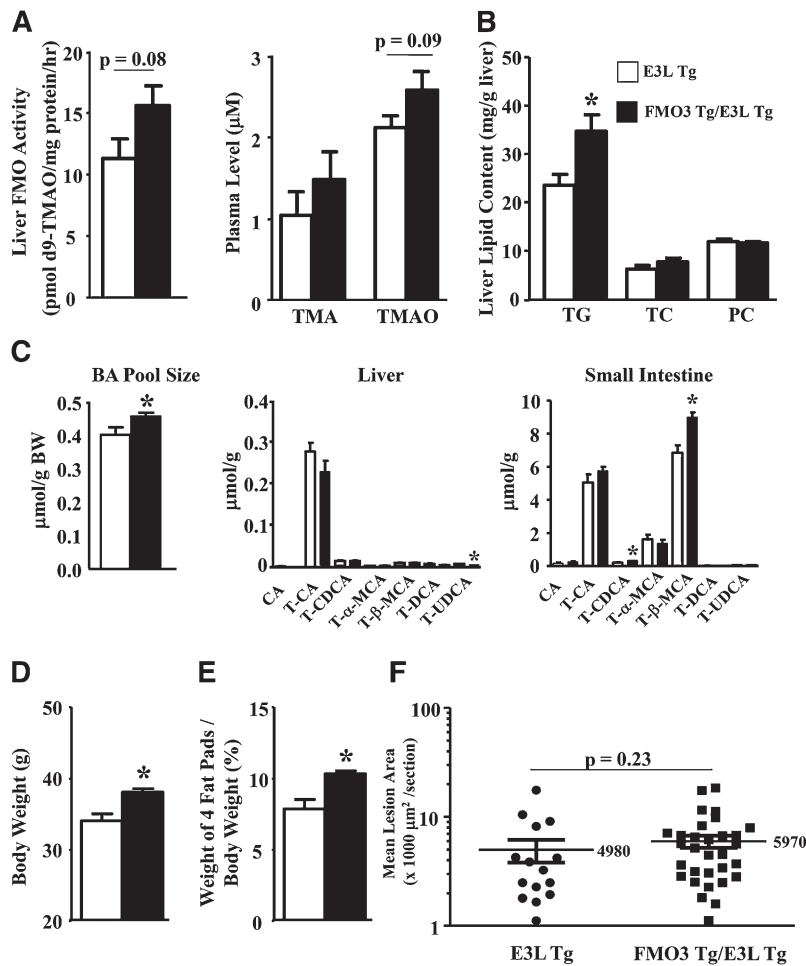


Fig. 8. FMO3 overexpression in Tg mice influences liver FMO activity, plasma TMAO, hepatic lipid content, bile acid pool size and composition, body weight, adiposity, and atherosclerotic lesion size. FMO3 Tg/E3L Tg and E3L Tg mice were fed the HF/HC diet for 16 weeks prior to tissue collection. Liver FMO activity ($n = 7$ for each group) and plasma TMA and TMAO levels ($n = 8$ to 11 for each group) (A); hepatic levels ($n = 10$ for each group) of TG, TC, and phosphatidylcholine (PC) (B); and bile acid (BA) pool size and composition ($n = 7$ to 10 for each group) (C) were measured. For bile acid composition, only the major ($\geq 0.5\%$ of total amount) bile acid species are plotted. Body weight (D) and percent weight (E) of four fat pads (gonadal, retroperitoneal, subcutaneous, and mesentery fat pads), normalized by the body weight, were determined ($n = 9$ to 12 for each group). F: Mean atherosclerotic lesion sizes at the aortic root region were quantified ($n = 15$ for E3L Tg, $n = 31$ for FMO3 Tg/E3L Tg). The lesion data were logarithmically transformed for the t -test. Student's t -test: * $P < 0.05$ as compared with the E3L Tg mice.

Ad-CMV-infected cells (Fig. 9A, left panel). The FMO activity was increased by 14-fold in the Ad-FMO3-infected cells as well (Fig. 9A, right panel). The glucose secretion rate of the Ad-FMO3-infected cells was increased by $\sim 80\%$ as compared with that of the Ad-CMV-infected cells (Fig. 9B) when the cells were incubated with a glucose-free media that promotes gluconeogenesis. In addition, the Ad-FMO3-infected cells exhibited a 43% increase in lipogenesis as determined by incorporation of ^{14}C -acetate into cellular lipids including free fatty acid, phospholipid, TG, cholesterol, and cholesteryl ester, as compared with the Ad-CMV-infected cells (Fig. 9C). Interestingly, the mRNA levels of genes involved in gluconeogenesis, such as ALT, G6PC, and PEPCK, were significantly elevated in the Ad-FMO3-infected cells (Fig. 9D). The expression of OTC, a gene involved in the urea cycle, was also significantly increased in the Ad-FMO3-infected cells as compared with the Ad-CMV-infected cells (Fig. 9D). Our data suggest that FMO3 overexpression is associated with increased expression of genes involved in gluconeogenesis. The mRNA levels of several genes involved in lipogenesis, including SREBP-1c, a transcription factor that controls the expression of lipogenesis genes, FASN, and stearoyl-CoA desaturase (SCD), were similar between the Ad-FMO3- and Ad-CMV-infected cells (data not shown). Therefore, FMO3 overexpression in cell culture did not directly increase the expression of genes involved in lipogenesis. The increased

lipogenesis we observed in Ad-FMO3-infected cells (Fig. 9C) might have been caused by increased availability of glucose in these cells, leading to elevated acetyl-CoA, the precursor for fatty acid synthesis.

Associations between plasma TMAO levels, lipid levels, and atherosclerosis resulting from natural variation among inbred strains of mice

Our FMO3 knockdown and overexpression studies suggest a role for FMO3 in modulating plasma lipoprotein levels in mice. We have, therefore, explored whether common functional variations of FMO3 in mice might also influence plasma lipid traits. We previously reported a significant *cis*-expression quantitative trait locus ($P = 1.78 \times 10^{-6}$) located in the *Fmo3* gene (SNP rs30760034, located in Chr. 1, 164896447 bp) that controls the hepatic FMO3 mRNA levels among a panel of ~ 100 different inbred strains of mice (30). Indeed, in this same panel, significant associations were observed between plasma lipid traits (including VLDL/IDL/LDL-cholesterol, total, HDL-cholesterol, and unesterified cholesterol) and SNPs located in a region of mouse chromosome 1 within 1 Mb of the *Fmo3* locus (supplementary Table 5).

Furthermore, we previously observed that atherosclerotic lesion size was significantly correlated with both plasma lipid and TMAO levels among 22 inbred strains of apoB Tg/HMDP mice (1, 23). We performed biweight

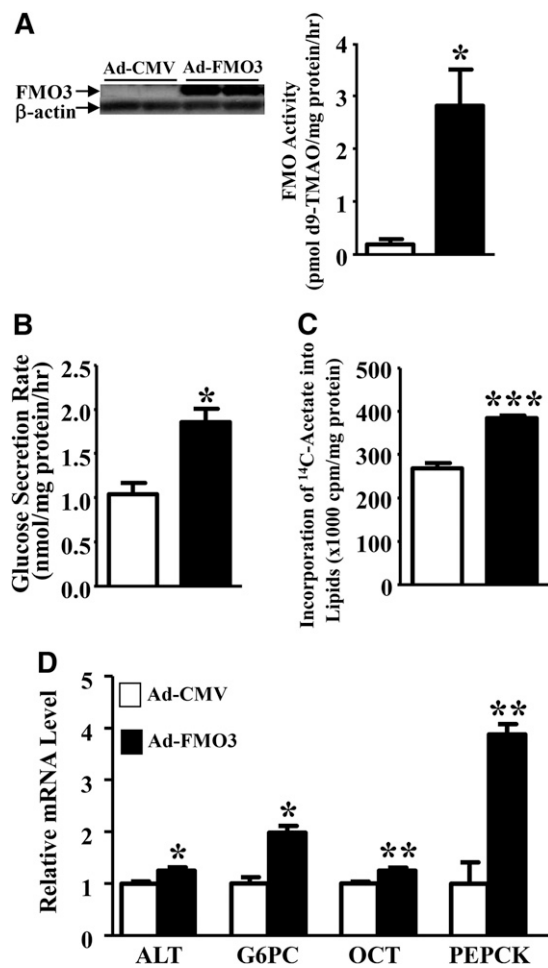


Fig. 9. FMO3 overexpression in Hep3B cells leads to increased glucose production and lipogenesis. Hep3B cells were infected with Ad-CMV or Ad-FMO3 for 2 days, and FMO3 protein levels ($n = 4$ for each group, left panel) and FMO activity ($n = 3$ for each group, right panel) (A), glucose secretion rates (B), lipogenesis rates (C), and mRNA levels (D) were measured. For B–D, $n = 4$ to 6 for each group. Student's *t*-test: * $P < 0.05$, ** $P < 0.01$, and *** $P < 0.0001$ as compared with the Ad-CMV group, respectively.

midcorrelation analyses of these data to examine the pairwise relationships between plasma TMAO, HDL-cholesterol, and VLDL/IDL/LDL-cholesterol levels, as well as atherosclerotic lesion size among the 22 strains of apoB Tg/HMDP mice (133 female mice) (supplementary Table 6A). We observed a moderate but significant positive correlation between TMAO and VLDL/IDL/LDL levels and an inverse correlation between TMAO and HDL levels (supplementary Table 6A). The positive association between TMAO and VLDL/IDL/LDL levels is consistent with our results because FMO3 knockdown led to decreases in both TMAO and VLDL/IDL/LDL-cholesterol levels, whereas FMO3 overexpression increased both. The inverse correlation between TMAO and HDL-cholesterol levels suggests that there are additional factors, other than FMO3, that have effects on HDL-cholesterol levels in the set of mouse strains. Moreover, we observed significant associations between atherosclerotic lesion size and plasma levels of TMAO, HDL-cholesterol, and VLDL/

IDL/LDL-cholesterol (supplementary Table 6A), with the order of association: VLDL/IDL/LDL cholesterol > HDL cholesterol > TMAO. To estimate the relative importance of these factors in atherosclerosis development in mice, we performed stepwise linear regression analysis (supplementary Table 6B). The analysis showed that among these three factors, VLDL/IDL/LDL-cholesterol was the most important predictor of lesion size, followed by HDL-cholesterol and then TMAO (supplementary Table 6B).

We conclude that common natural variations perturbing expression of FMO3 in mice influence plasma lipid levels as well as TMA/TMAO levels.

DISCUSSION

We began this study to test whether inhibition of FMO3 would reduce atherosclerosis in hyperlipidemic mouse models, providing a possible approach to human therapy for the disease. We were surprised to discover that perturbation of FMO3 expression has profound effects on lipid and glucose metabolism, as well as potential proinflammatory effects. Hepatic gene expression analysis revealed significantly decreased expression of genes involved in gluconeogenesis and lipogenesis in the FMO3 ASO-treated mice as compared with the control mice, providing a molecular basis for the lower lipid and glucose levels seen in these mice. These results reveal a novel role of FMO3, and possibly TMA/TMAO, in lipid and glucose metabolism. Clearly, efforts to modulate TMAO levels for therapeutic purposes by targeting FMO3 will have to consider these metabolic effects.

We observed that FMO3-specific ASO knockdown in LDLRKO mice led to 90% decreases in hepatic FMO3 protein and FMO3 activity levels and resulted in significant decreases in plasma levels of TMAO and atherosclerosis. In addition, we observed decreased levels of plasma lipids, glucose, insulin, and ketone bodies, as well as concomitant increases in plasma levels of glucogenic and ketogenic amino acids, suggesting decreased hepatic gluconeogenesis and ketogenesis. Hepatic glucose and lipid levels were also significantly decreased in the FMO3 ASO-treated mice. Treatment of female and male B6 mice by two independent FMO3-specific ASOs led to similar decreases in plasma lipids, glucose, and insulin levels, suggesting that the observed metabolic changes associated with the FMO3 ASO treatment were caused by FMO3 deficiency rather than a nonspecific effect. Using a complementary approach, we found that FMO3 overexpression in Tg mice led to moderate but significant increases in liver FMO activity and significant increases in plasma lipid levels, hepatic TG content, and adiposity. There was a trend of increased plasma glucose and insulin levels and increased atherosclerosis in FMO3 Tg mice as well.

The lipid and glucose changes observed in our studies in response to perturbations of FMO3 are not likely to be mediated by TMAO because elevated TMAO levels caused by dietary supplementation of TMAO, L-carnitine, or choline did not lead to significant changes in plasma TG,

cholesterol, lipoprotein, or glucose levels, or hepatic TG or cholesterol levels in apoE null (ApoEKO) mice (2, 3). On the other hand, in a study using male C57BL/6J mice, TMAO supplementation was associated with significantly decreased plasma TG and TC levels, the opposite of our findings, and increased insulin levels (31). Moreover, overexpression of FMO3 in Hep3B cells by adenovirus-mediated gene transduction led to significantly increased glucose production and lipogenesis, suggesting a direct role for FMO3 in modulating lipid and glucose homeostasis. While TMA/TMAO may explain some of the effects on lipids and glucose metabolism, we feel the data are most consistent with the concept that FMO3 modulates the hepatic level(s) of an unknown physiological substrate(s), which, in turn, influences lipid and glucose metabolism in the liver.

The decreased lipogenesis we observed in the livers of FMO3 ASO-treated mice could be the result of decreased insulin levels. Insulin regulates liver lipogenesis through a series of signaling steps that activate SREBP-1c (32–37), which in turn increases the expression of lipogenic genes such as *Fasn* and *Scd-1*. We observed decreased hepatic expression of SREBP-1c and lipogenesis genes in the FMO3 ASO-treated mice, consistent with decreased insulin levels.

Our data revealed decreased hepatic gluconeogenesis in the FMO3 ASO-treated mice. Hepatic gluconeogenesis is closely regulated by the opposing actions of insulin and glucagon. In a fed state, insulin inhibits gluconeogenesis through AKT (also known as protein kinase B)-mediated phosphorylation of the transcription factor FOXO1, leading to its nuclear exclusion and degradation (38). In the fasting state, glucagon stimulates gluconeogenesis by multiple pathways, leading to increased expression of FOXO1, G6PC, and PEPCK (39, 40). We observed decreased levels of FOXO1 in the FMO3 ASO-treated mice. However, we did not observe significant differences in circulating glucagon levels between the FMO3 ASO-treated and the control mice.

In an attempt to understand the mechanism by which FMO3 expression is linked to lipid and glucose metabolism, we carried out global microarray expression analyses. The studies revealed that FMO3 knockdown is associated with a preferentially decreased expression of PPAR α and its target genes in the liver, possibly due to reduced hepatic concentrations of PPAR α ligands, including palmitoleate, oleate, α - or γ -linolenate, and EPA (Fig. 7D). Both linolenate and EPA are essential fatty acids derived entirely from dietary sources. Because there was no difference in the daily fecal TG output between the mice treated with FMO3 or control ASO (Fig. 6D), it is unlikely that FMO3 knockdown impaired the intestinal absorption of essential fatty acids. However, FMO3 may modulate the catabolism of these unsaturated fatty acids and indirectly influence the activation of PPAR α . PPAR α is activated during fasting and stimulates fatty acid oxidation, ketogenesis, and gluconeogenesis through transactivation of its target genes (21) and thus could explain many of the observed effects of the FMO3 perturbation. PPAR α also regulates

genes involved in bile acid synthesis, including *Cyp7a1* and *Cyp8b1* (21, 41), and plays a role in modulating inflammatory responses in the artery wall and liver by interference with the nuclear factor κ B (NF- κ B) pathway through direct binding to p65 (42) and other mechanisms (43, 44).


The microarray data also revealed decreased expression of *Klf15* and some of its target genes in the livers of FMO3 ASO-treated mice. Recent studies have shown the importance of KLF15 in modulating gluconeogenesis, amino acid degradation, and urea cycle (26–28). Moreover, KLF15 regulates inflammation by altering the acetylation status and activity of NF- κ B through direct interaction with p300 (45). Thus, the increased hepatic inflammation we observed in the FMO3 ASO-treated mice might have been caused by impaired PPAR α and KLF15 activities.

Previously, dietary TMAO supplementation was shown to decrease bile acid pool size in ApoEKO mice (2). In contrast, we observed decreased TMAO levels and decreased bile acid pool sizes in FMO3 ASO-treated LDLRKO mice. Furthermore, FMO3 overexpression led to increased bile acid pool size (Fig. 8C) in the FMO3 Tg mice. These results suggest that FMO3 influences bile acid homeostasis through pathways other than TMAO. The observed changes in bile acid metabolism could be linked to the inflammatory effects in liver. Specifically, TNF α has been previously demonstrated to decrease the expression of *Cyp7a1* through activation of the MAPK pathway (46). Moreover, decreased *Cyp7a1* and *Cyp8b1* expression due to reduced transactivation by PPAR α in the livers of FMO3 ASO-treated mice probably contributed to the decreased bile acid pool size as well.

Our study suggests a role for FMO3 in modulating adiposity as well because FMO3 knockdown and overexpression lead to significantly decreased and increased adiposity, respectively. This could be modulated in part by the effects of FMO3 on plasma TG and glucose levels. Thus, lower plasma TG and glucose levels in the FMO3 ASO-treated LDLRKO mice lead to lower TG accumulation and decreased fat pad weight/adiposity, whereas the opposite is true in the FMO3 Tg mice.

Our results in mice suggest that naturally occurring subtle variations in FMO3 expression can significantly perturb lipid metabolism as well as TMA/TMAO levels. Thus, we observed that among different inbred strains of mice, plasma lipid levels mapped to the region of the *Fmo3* gene and that TMAO levels were significantly correlated with plasma lipid levels. This raises the possibility that common variations of the FMO3 gene in human populations may also affect lipid or glucose metabolism and that these could explain, in part, the observed correlations between TMAO level and atherosclerosis. This does not appear to be the case, however, because plasma lipids were not correlated with TMAO in human studies, and neither TMAO levels nor lipid levels were associated with the *FMO3* gene in a genome-wide association study (9). Perhaps common variations in FMO3 expression or activity do not occur in the human populations that were studied. Alternatively, there may be differences between mice and humans in the metabolic interactions of FMO3. The recessive disorder

trimethylaminuria, due to loss of function mutations of *FMO3* gene, occurs at a frequency of ~1 in 10,000 in Caucasian populations (4). It will be of interest to examine whether these individuals or obligate heterozygous individuals exhibit alterations in lipid and glucose metabolism.

In summary, we uncovered a novel role for *FMO3* in modulating glucose and lipid homeostasis in vivo. Our findings suggest that *FMO3* modulates lipid and glucose in a dose-dependent manner and that these effects are most likely independent of TMA/TMAO metabolism. Whether the underlying mechanism involves unknown catalytic activities of *FMO3* or regulatory functions distinct from its catalytic activity is unknown. However, our data revealed that *FMO3* influences the activities of two master regulators of hepatic metabolite homeostasis and inflammation, namely PPAR α and KLF15. 

The authors thank Zhiqiang Zhou, Kathy Kampf, and Melenie Rosales for excellent technical assistance and Dr. Rita Cantor for advice on statistical analysis.

REFERENCES

- Bennett, B. J., T. Q. de Aguiar Vallim, Z. Wang, D. M. Shih, Y. Meng, J. Gregory, H. Allayee, R. Lee, M. Graham, R. Crooke, et al. 2013. Trimethylamine-N-oxide, a metabolite associated with atherosclerosis, exhibits complex genetic and dietary regulation. *Cell Metab.* **17**: 49–60.
- Koeth, R. A., Z. Wang, B. S. Levison, J. A. Buffa, E. Org, B. T. Sheehy, E. B. Britt, X. Fu, Y. Wu, L. Li, et al. 2013. Intestinal microbiota metabolism of L-carnitine, a nutrient in red meat, promotes atherosclerosis. *Nat. Med.* **19**: 576–585.
- Wang, Z., E. Klipfell, B. J. Bennett, R. Koeth, B. S. Levison, B. Dugar, A. E. Feldstein, E. B. Britt, X. Fu, Y. M. Chung, et al. 2011. Gut flora metabolism of phosphatidylcholine promotes cardiovascular disease. *Nature.* **472**: 57–63.
- Phillips, I. R., and E. A. Shephard. 2008. Flavin-containing monooxygenases: mutations, disease and drug response. *Trends Pharmacol. Sci.* **29**: 294–301.
- Zhou, J., and E. A. Shephard. 2006. Mutation, polymorphism and perspectives for the future of human flavin-containing monooxygenase 3. *Mutat. Res.* **612**: 165–171.
- Treacy, E. P., B. R. Akerman, L. M. Chow, R. Youil, C. Bibeau, J. Lin, A. G. Bruce, M. Knight, D. M. Danks, J. R. Cashman, et al. 1998. Mutations of the flavin-containing monooxygenase gene (*FMO3*) cause trimethylaminuria, a defect in detoxication. *Hum. Mol. Genet.* **7**: 839–845.
- Dolan, C., D. C. Shields, A. Stanton, E. O'Brien, D. M. Lambert, J. K. O'Brien, and E. P. Treacy. 2005. Polymorphisms of the Flavin containing monooxygenase 3 (*FMO3*) gene do not predispose to essential hypertension in Caucasians. *BMC Med. Genet.* **6**: 41.
- Tang, W. H., Z. Wang, B. S. Levison, R. A. Koeth, E. B. Britt, X. Fu, Y. Wu, and S. L. Hazen. 2013. Intestinal microbial metabolism of phosphatidylcholine and cardiovascular risk. *N. Engl. J. Med.* **368**: 1575–1584.
- Hartiala, J., B. J. Bennett, W. H. Tang, Z. Wang, A. F. Stewart, R. Roberts, R. McPherson, A. J. Lusis, S. L. Hazen, and H. Allayee. 2014. Comparative genome-wide association studies in mice and humans for trimethylamine N-oxide, a proatherogenic metabolite of choline and L-carnitine. *Arterioscler. Thromb. Vasc. Biol.* **34**: 1307–1313.
- Ishibashi, S., J. L. Goldstein, M. S. Brown, J. Herz, and D. K. Burns. 1994. Massive xanthomatosis and atherosclerosis in cholesterol-fed low density lipoprotein receptor-negative mice. *J. Clin. Invest.* **93**: 1885–1893.
- van den Maagdenberg, A. M., M. H. Hofker, P. J. Krimpenfort, I. de Bruijn, B. van Vlijmen, H. van der Boom, L. M. Havekes, and R. R. Frants. 1993. Transgenic mice carrying the apolipoprotein E3-Leiden gene exhibit hyperlipoproteinemia. *J. Biol. Chem.* **268**: 10540–10545.
- Koller, E., T. M. Vincent, A. Chappell, S. De, M. Manoharan, and C. F. Bennett. 2011. Mechanisms of single-stranded phosphorothioate modified antisense oligonucleotide accumulation in hepatocytes. *Nucleic Acids Res.* **39**: 4795–4807.
- Mehrabian, M., J. H. Qiao, R. Hyman, D. Ruddle, C. Laughton, and A. J. Lusis. 1993. Influence of the apoA-II gene locus on HDL levels and fatty streak development in mice. *Arterioscler. Thromb.* **13**: 1–10.
- Folch, J., M. Lees, and G. H. Sloane Stanley. 1957. A simple method for the isolation and purification of total lipides from animal tissues. *J. Biol. Chem.* **226**: 497–509.
- Shih, D. M., Z. Shaposhnik, Y. Meng, M. Rosales, X. Wang, J. Wu, B. Ratiner, F. Zadini, G. Zadini, and A. J. Lusis. 2013. Hyodeoxycholic acid improves HDL function and inhibits atherosclerotic lesion formation in LDLR-knockout mice. *FASEB J.* **27**: 3805–3817.
- Argmann, C. A., S. M. Houten, M-F. Champy, and J. Auwerx. 2006. Lipid and bile acid analysis. *Curr. Protoc. Mol. Biol.* **75**: 29B.2.1–29B.2.24.
- Ghazalpour, A., B. J. Bennett, D. Shih, N. Che, L. Orozco, C. Pan, R. Hagopian, A. He, P. Kayne, W. P. Yang, et al. 2014. Genetic regulation of mouse liver metabolite levels. *Mol. Syst. Biol.* **10**: 730.
- Millar, J. S., D. A. Cromley, M. G. McCoy, D. J. Rader, and J. T. Billheimer. 2005. Determining hepatic triglyceride production in mice: comparison of poloxamer 407 with Triton WR-1339. *J. Lipid Res.* **46**: 2023–2028.
- Castellani, L. W., M. Navab, B. J. Van Lenten, C. C. Hedrick, S. Y. Hama, A. M. Goto, A. M. Fogelman, and A. J. Lusis. 1997. Overexpression of apolipoprotein AII in transgenic mice converts high density lipoproteins to proinflammatory particles. *J. Clin. Invest.* **100**: 464–474.
- Rakhshandehroo, M., L. M. Sanderson, M. Matilainen, R. Stienstra, C. Carlberg, P. J. de Groot, M. Muller, and S. Kersten. 2007. Comprehensive analysis of PPARalpha-dependent regulation of hepatic lipid metabolism by expression profiling. *PPAR Res.* **2007**: 26839.
- Kersten, S. 2014. Integrated physiology and systems biology of PPARalpha. *Mol. Metab.* **3**: 354–371.
- Orozco, L. D., M. H. Kapturczak, B. Barajas, X. Wang, M. M. Weinstein, J. Wong, J. Deshane, S. Bolisetty, Z. Shaposhnik, D. M. Shih, et al. 2007. Heme oxygenase-1 expression in macrophages plays a beneficial role in atherosclerosis. *Circ. Res.* **100**: 1703–1711.
- Bennett, B. J., L. Orozco, E. Kostem, A. Erbilgin, M. Dallinga, I. Neuhaus, B. Guan, X. Wang, E. Eskin, and A. J. Lusis. 2012. High-resolution association mapping of atherosclerosis loci in mice. *Arterioscler. Thromb. Vasc. Biol.* **32**: 1790–1798.
- Patra, C. R., S. S. Abdel Moneim, E. Wang, S. Dutta, S. Patra, M. Eshed, P. Mukherjee, A. Gedanken, V. H. Shah, and D. Mukhopadhyay. 2009. In vivo toxicity studies of europium hydroxide nanorods in mice. *Toxicol. Appl. Pharmacol.* **240**: 88–98.
- Potthoff, M. J., T. Inagaki, S. Satapati, X. Ding, T. He, R. Goetz, M. Mohammadi, B. N. Finck, D. J. Mangelsdorf, S. A. Kliewer, et al. 2009. FGF21 induces PGC-1alpha and regulates carbohydrate and fatty acid metabolism during the adaptive starvation response. *Proc. Natl. Acad. Sci. USA.* **106**: 10853–10858.
- Jeyaraj, D., F. A. Scheer, J. A. Ripperger, S. M. Haldar, Y. Lu, D. A. Prosdocimo, S. J. Eapen, B. L. Eapen, Y. Cui, G. H. Mahabeshwar, et al. 2012. Klf15 orchestrates circadian nitrogen homeostasis. *Cell Metab.* **15**: 311–323.
- Gray, S., B. Wang, Y. Orihuela, E. G. Hong, S. Fisch, S. Haldar, G. W. Cline, J. K. Kim, O. D. Peroni, B. B. Kahn, et al. 2007. Regulation of gluconeogenesis by Kruppel-like factor 15. *Cell Metab.* **5**: 305–312.
- Takashima, M., W. Ogawa, K. Hayashi, H. Inoue, S. Kinoshita, Y. Okamoto, H. Sakaue, Y. Wataoka, A. Emi, Y. Senga, et al. 2010. Role of KLF15 in regulation of hepatic gluconeogenesis and metformin action. *Diabetes.* **59**: 1608–1615.
- Chen, F., L. Ma, P. A. Dawson, C. J. Sinal, E. Sehayek, F. J. Gonzalez, J. Breslow, M. Ananthanarayanan, and B. L. Schneider. 2003. Liver receptor homologue-1 mediates species- and cell line-specific bile acid-dependent negative feedback regulation of the apical sodium-dependent bile acid transporter. *J. Biol. Chem.* **278**: 19909–19916.
- Bennett, B. J., C. R. Farber, L. Orozco, H. M. Kang, A. Ghazalpour, N. Siemers, M. Neubauer, I. Neuhaus, R. Yordanova, B. Guan, et al. 2010. A high-resolution association mapping panel for the dissection of complex traits in mice. *Genome Res.* **20**: 281–290.
- Gao, X., X. Liu, J. Xu, C. Xue, Y. Xue, and Y. Wang. 2014. Dietary trimethylamine N-oxide exacerbates impaired glucose tolerance in mice fed a high fat diet. *J. Biosci. Bioeng.* **118**: 476–481.
- Repa, J. J., G. Liang, J. Ou, Y. Bashmakov, J. M. Lobaccaro, I. Shimomura, B. Shan, M. S. Brown, J. L. Goldstein, and D. J.

- Mangelsdorf. 2000. Regulation of mouse sterol regulatory element-binding protein-1c gene (SREBP-1c) by oxysterol receptors, LXRalpha and LXRbeta. *Genes Dev.* **14**: 2819–2830.
33. Chen, G., G. Liang, J. Ou, J. L. Goldstein, and M. S. Brown. 2004. Central role for liver X receptor in insulin-mediated activation of Srebp-1c transcription and stimulation of fatty acid synthesis in liver. *Proc. Natl. Acad. Sci. USA.* **101**: 11245–11250.
 34. Bakan, I., and M. Laplante. 2012. Connecting mTORC1 signaling to SREBP-1 activation. *Curr. Opin. Lipidol.* **23**: 226–234.
 35. Saliel, A. R., and C. R. Kahn. 2001. Insulin signalling and the regulation of glucose and lipid metabolism. *Nature.* **414**: 799–806.
 36. Li, S., M. S. Brown, and J. L. Goldstein. 2010. Bifurcation of insulin signaling pathway in rat liver: mTORC1 required for stimulation of lipogenesis, but not inhibition of gluconeogenesis. *Proc. Natl. Acad. Sci. USA.* **107**: 3441–3446.
 37. Porstmann, T., C. R. Santos, B. Griffiths, M. Cully, M. Wu, S. Leever, J. R. Griffiths, Y. L. Chung, and A. Schulze. 2008. SREBP activity is regulated by mTORC1 and contributes to Akt-dependent cell growth. *Cell Metab.* **8**: 224–236.
 38. Nakae, J., B. C. Park, and D. Accili. 1999. Insulin stimulates phosphorylation of the forkhead transcription factor FKHR on serine 253 through a Wortmannin-sensitive pathway. *J. Biol. Chem.* **274**: 15982–15985.
 39. Cheng, Z., and M. F. White. 2011. Targeting Forkhead box O1 from the concept to metabolic diseases: lessons from mouse models. *Antioxid. Redox Signal.* **14**: 649–661.
 40. Wondisford, A. R., L. Xiong, E. Chang, S. Meng, D. J. Meyers, M. Li, P. A. Cole, and L. He. 2014. Control of Foxo1 gene expression by co-activator P300. *J. Biol. Chem.* **289**: 4326–4333.
 41. Hunt, M. C., Y. Z. Yang, G. Eggertsen, C. M. Carneheim, M. Gafvels, C. Einarsson, and S. E. Alexson. 2000. The peroxisome proliferator-activated receptor alpha (PPARalpha) regulates bile acid biosynthesis. *J. Biol. Chem.* **275**: 28947–28953.
 42. Delerive, P., K. De Bosscher, S. Besnard, W. Vanden Berghe, J. M. Peters, F. J. Gonzalez, J. C. Fruchart, A. Tedgui, G. Haegeman, and B. Staels. 1999. Peroxisome proliferator-activated receptor alpha negatively regulates the vascular inflammatory gene response by negative cross-talk with transcription factors NF-kappaB and AP-1. *J. Biol. Chem.* **274**: 32048–32054.
 43. Zambon, A., P. Gervois, P. Paultet, J. C. Fruchart, and B. Staels. 2006. Modulation of hepatic inflammatory risk markers of cardiovascular diseases by PPAR-alpha activators: clinical and experimental evidence. *Arterioscler. Thromb. Vasc. Biol.* **26**: 977–986.
 44. De Bosscher, K., W. Vanden Berghe, and G. Haegeman. 2006. Cross-talk between nuclear receptors and nuclear factor kappaB. *Oncogene.* **25**: 6868–6886.
 45. Lu, Y., L. Zhang, X. Liao, P. Sangwung, D. A. Prosdocimo, G. Zhou, A. R. Votruba, L. Brian, Y. J. Han, H. Gao, et al. 2013. Kruppel-like factor 15 is critical for vascular inflammation. *J. Clin. Invest.* **123**: 4232–4241.
 46. De Fabiani, E., N. Mitro, A. C. Anzulovich, A. Pinelli, G. Galli, and M. Crestani. 2001. The negative effects of bile acids and tumor necrosis factor-alpha on the transcription of cholesterol 7alpha-hydroxylase gene (CYP7A1) converge to hepatic nuclear factor-4: a novel mechanism of feedback regulation of bile acid synthesis mediated by nuclear receptors. *J. Biol. Chem.* **276**: 30708–30716.